

pubs.acs.org/JACS Article

Spatial Heterogeneity of Biexcitons in Two-Dimensional Ruddlesden-Popper Lead Iodide Perovskites

Zachary T. Armstrong, Kristel M. Forlano, Chris R. Roy, Miriam Bohlmann Kunz, Kieran Farrell, Dongxu Pan, John C. Wright, Song Jin,* and Martin T. Zanni*



Cite This: J. Am. Chem. Soc. 2023, 145, 18568-18577



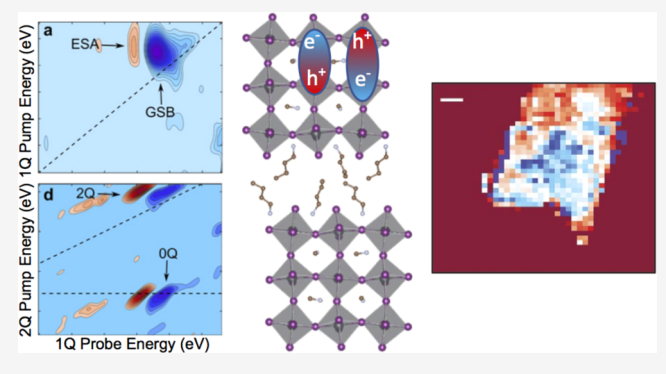
ACCESS

III Metrics & More

Article Recommendations

s Supporting Information

ABSTRACT: Quantum confinement in two-dimensional (2D) Ruddlesden–Popper (RP) perovskites leads to the formation of stable quasi-particles, including excitons and biexcitons, the latter of which may enable lasing in these materials. Due to their hybrid organic—inorganic structures and the solution phase synthesis, microcrystals of 2D RP perovskites can be quite heterogeneous, with variations in excitonic and biexcitonic properties between crystals from the same synthesis and even within individual crystals. Here, we employ one- and two-quantum two-dimensional whitelight microscopy to systematically study the spatial variations of excitons and biexcitons in microcrystals of a series of 2D RP perovskites $BA_2MA_{n-1}Pb_nI_{3n+1}$ (n=2-4, BA= butylammonium, AA= methylammonium). We find that the average biexciton



binding energy of around 60 meV is essentially independent of the perovskite layer thickness (n). We also resolve spatial variations of the exciton and biexciton energies on micron length scales within individual crystals. By comparing the one-quantum and two-quantum spectra at each pixel, we conclude that biexcitons are more sensitive to their environments than excitons. These results shed new light on the ways disorder can modify the energetic landscape of excitons and biexcitons in RP perovskites and how biexcitons can be used as a sensitive probe of the microscopic environment of a semiconductor.

■ INTRODUCTION

Two-dimensional (2D) Ruddlesden-Popper (RP) halide perovskites¹⁻⁴ are a class of materials that host a plethora of optical and quantum phenomena including broadband emission, 5,6 strong electron—phonon coupling, 7–9 lasing, 10–12 and stable quasi-particle states including trions and biexcitons. 13-15 The structure of RP perovskites consists of quasi-2D perovskite-like slabs of corner-sharing octahedra separated by bilayers of large organic spacer cations like *n*-butylammonium (BA) (Figure 1a) or phenethylammonium (PEA). The thickness of the perovskite slabs (in units of PbX₆²⁻ octahedra) is indexed by the coefficient n in the RP perovskite chemical formula $(LA)_2(A)_{n-1}Pb_nX_{3n+1}$. The RP perovskite materials considered here have the formula: $BA_2MA_{n-1}Pb_nI_{3n+1}$, where BA is the spacer cation and MA is methylammonium, the "A" site cation residing in the cavities in the octahedral layers. Many other compositions are possible, including other spacer cations, A cations, 16-18 and mixed halide compositions, 19,20 all of which will affect the optoelectronic properties. Quantum confinement of charge carriers in the octahedral layers leads to several phenomena including stable excitons at room temperature.21 The exciton binding energy scales inversely with n, increasing from <10 meV (at 300 K) in 3D lead iodide perovskites²² to >400 meV at the 2D n = 1 limit.²¹ It is well

known that 2D perovskites often exhibit spatial heterogeneity, ^{23–26} which can influence carrier dynamics and optoelectronic device operation. ^{27,28} Their soft lattice ^{29,30} also leads to strong disorder, ^{31,32} which has been examined in the context of carrier localization and relaxation. However, many of these prior studies lack sufficient spatial resolution with spectral specificity to disentangle how various sources of disorder and heterogeneity impact the electronic structure of excitons and other carriers in 2D perovskites.

Moreover, 2D perovskites exhibit both strong electron—phonon^{8,33-36} and spin—orbit couplings.³⁷⁻³⁹ These interactions, combined with high quantum confinement relative to 3D perovskites, result in a complicated electronic structure. While there is a good understanding^{40,41} of the excitonic features of this class of materials, many open questions remain about the properties of higher-order many-body states. Biexcitons have been reported in perovskite nanocryst-

Received: May 26, 2023 Published: August 11, 2023





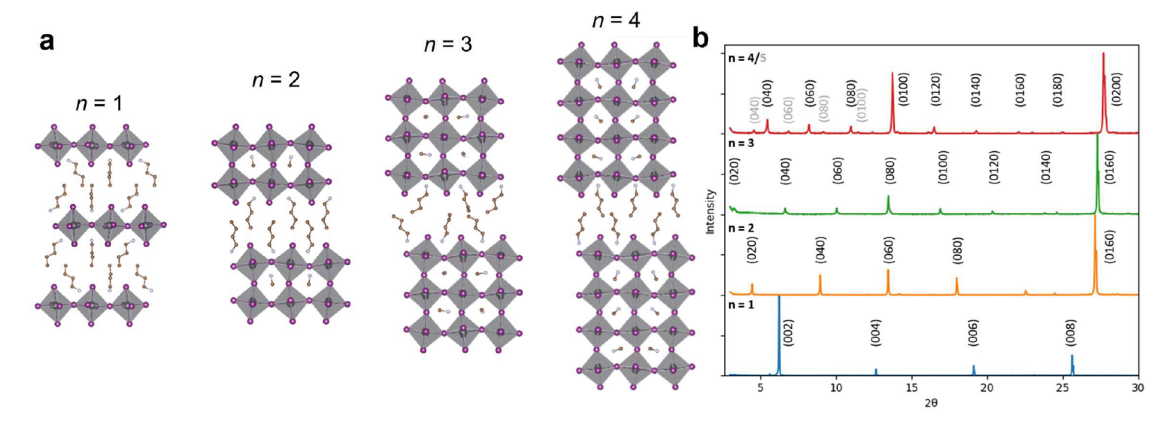


Figure 1. (a) Structures of n = 1-4 2D RP perovskites and (b) powder X-ray diffraction patterns of the BA₂MA_{n-1}Pb_nI_{3n+1} (n = 1-4) microcrystal samples studied herein. Powder sample for n = 4 contained some n = 5 impurity, peaks labeled in light gray.

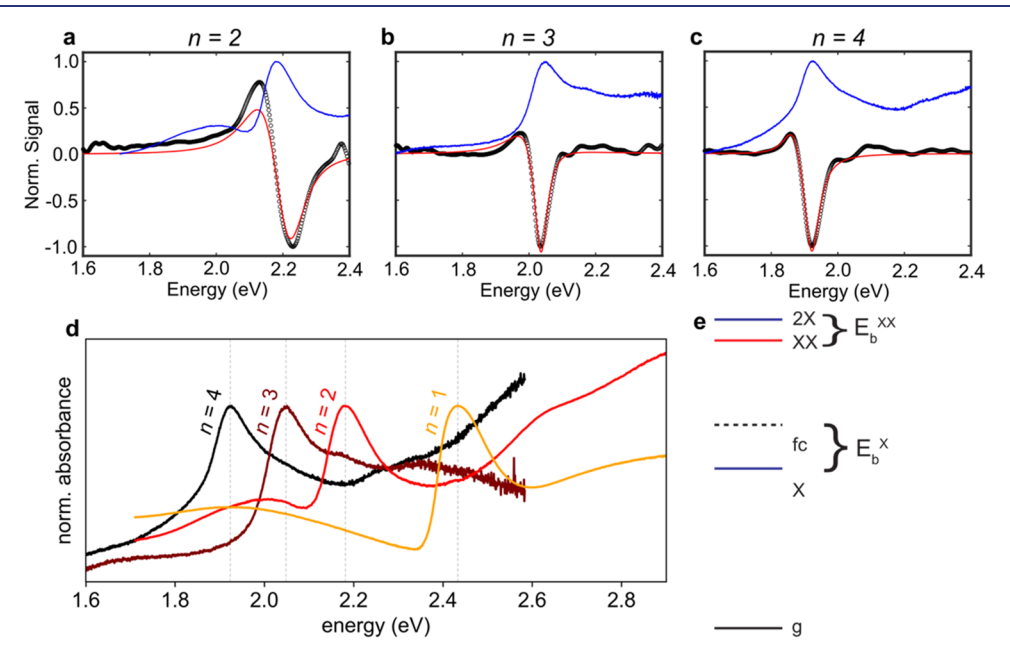


Figure 2. Broadband TA spectra of excitons and biexcitons at zero delay from submicron spots of n = 2 (a), n = 3 (b), and n = 4 (c) $BA_2MA_{n-1}Pb_nI_{3n+1}$ microcrystal samples. Experimental data is shown as black dots, and Lorentzian fits are shown as solid red lines. Linear absorption spectra for single microcrystals of the RP perovskite phases studied here are shown as blue lines in (a-c) and are compared in (d). Energy levels for excitons and biexcitons are illustrated in (e). The exciton binding energy (E_b^X) is measured with respect to the free carrier energy (fc), while the biexciton binding energy (E_b^{XX}) is measured with respect to twice the exciton energy.

als 14,42-44 and 2D perovskites, 13,15 but the nature of these quasi-particles remains poorly understood. Indeed, biexciton lasing has been reported in phenethylammonium-based 2D RP perovskites, but it is unclear if amplified spontaneous emission stems from biexcitons or from other states due to overlapping features in PL spectra. 12 A more detailed understanding of the types and properties of the quasi-particles found in 2D perovskites could help interpret ambiguous results from these studies. While biexcitons could serve as a platform for lasing in these materials, Auger recombination rates can be enhanced in a material that can host stable biexcitons, 45-47 meaning that the presence of biexcitons and their energetics can influence the relaxation processes of excitons and thus are important for improving the performance of optoelectronic devices such as light-emitting diodes and photovoltaic cells at high carrier densities. Higher n phases are important to consider because higher n phases have more and more free carrier character relative to exciton character, ^{21,48} and should at some point stop

hosting biexcitons.⁴¹ Higher *n* phase 2D perovskites also contain A cations that could influence the photophysical properties.

One particular topic of interest is how structural heterogeneity impacts the electronic structure of RP perovskites. Structural heterogeneity, including defects and varying degrees of crystallinity, can be difficult to control, ^{19,49,50} but can have drastic impacts on the relaxation dynamics of carriers. In addition to static structural heterogeneity or disorder, perovskites exhibit large amounts of dynamic disorder at room temperature. ^{13,31,32,51-53} This dynamic disorder can also impact carrier relaxation dynamics, and leads to a breakdown in understanding of the properties of RP perovskites when disorder is not considered. Ultrafast spectroscopy can be a sensitive probe of both static and dynamic disorder and their impact on the electronic structure and relaxation dynamics of carriers in semiconductors. ^{32,52,54} Spatially resolved ultrafast spectroscopy can further be leveraged to interrogate the

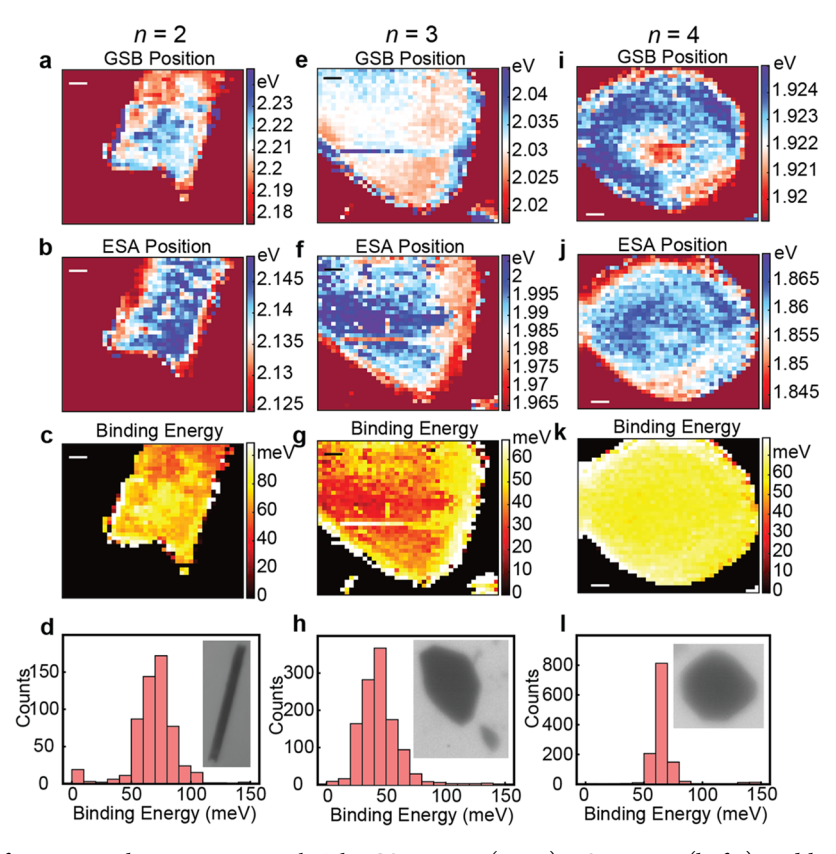


Figure 3. TA microscopy of BA₂MA_{n-1}Pb_nI_{3n+1} microcrystals. The GSB energy (a, e, i), ESA energy (b, f, j), and biexciton binding energy from Lorentzian fits (c, g, k) are shown as a function of position within a single microcrystal of n = 2 (a–), n = 3 (e–g), and n = 4 (i–k) perovskites. All scale bars are 2 μ m. Histograms of the biexciton binding energy are shown in (d, h, l), with optical microscope images of the microcrystals shown as insets.

structural heterogeneity present on micron length scales within individual microcrystals. $^{55-58}$

Here, we use transient absorption (TA) spectroscopy and microscopy, and two-dimensional white-light (2DWL) microscopy to systematically study a series of $BA_2MA_{n-1}Pb_nI_{3n+1}$ (n = 2-4) microcrystal samples to reveal the energetic landscapes of excitons and biexcitons in a spatially resolved manner for the first time. PL and TA spectroscopy reveals that biexcitons are stable at room temperature in n = 2-4 RP perovskites with an average binding energy of 60 meV, roughly independent of n. We use one- and two-quantum 2DWL spectroscopy to show that these biexcitons are hot biexcitons, as have been described in perovskite nanocrystals. 2DWL microscopy reveals that the average energies of the exciton and biexciton states vary by ~20 meV over micron length scales within each microcrystal as well as between individual microcrystals. These results shed new light on the role that disorder plays in setting the energetic environment of these materials.

RESULTS

The microcrystals of the series of 2D RP perovskites $BA_2MA_{n-1}Pb_nI_{3n+1}$ were grown on the surface of aqueous droplets of precursor solutions using a floating growth method we previously reported. Powder X-ray diffraction experiments (Figure 1b) confirmed the phase identity and purity of these microcrystal samples. These microcrystals can be transferred to glass substrates, and they have various shapes intrinsic to each phase due to their single-crystal nature and have typical lateral dimensions of $10-50~\mu m$ and thickness of 100-200~nm (Figure S1), meaning reabsorption effects are

suppressed. In Figure 2a, we show the broadband TA spectrum of a microcrystal of n = 2. We utilized a broadband pump pulse for both the TA and 2DWL measurements presented here. The white-light pump pulse covers the spectral range of 550-700 nm. There are two main features in the spectrum: a negative ground state bleach (GSB) from the 1s exciton at 2.227 eV and a positive excited state absorption (ESA) at 2.131 eV. The bleach position in the TA spectrum is consistent with the linear absorption spectrum (Figure 2d), confirming that this spectral feature is predominantly due to the bleach of the exciton state. The GSB and ESA transitions overlap, and we fit the spectrum with two Lorentzians to extract the precise peak positions. The fits to the spectrum are shown as solid lines in Figure 2a. The lower energy ESA has been assigned previously in 2D perovskites, 13,15 and many other materials, 59-62 as being from biexcitons. More details of the fitting procedure are given in the Supporting Information. The transition is from the exciton state to the doubly excited biexciton state, which is shifted from twice the energy of the exciton state by the binding energy (Figure 2e). Thus, this transition shows up at a lower energy than the GSB of the exciton and the energy difference between these two peaks is set by the biexciton binding energy. In the n = 2 spectrum shown in Figure 2a, this binding energy is 61.4 meV. Fits with three or four Lorenzians were conducted and were found to change the estimates of biexciton binding energy by no more than 20 meV. Similarly, fits with Gaussian lineshapes instead of Lorentzian lineshapes change the estimate of the biexciton binding energy by no more than 20 meV. No matter the fitting

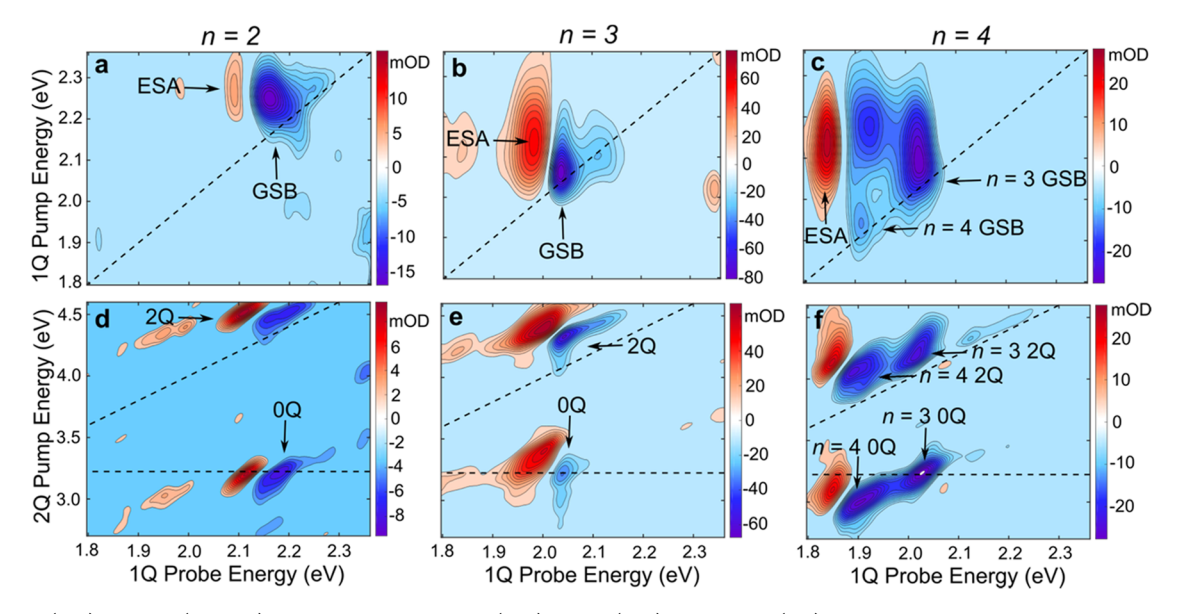


Figure 4. 1Q (top) and 2Q (bottom) 2DWL spectra of n = 2 (a, d), n = 3 (b, e), and n = 4. (c, f) BA₂MA_{n-1}Pb_nI_{3n+1} microcrystals collected from submicron spots within individual microcrystals at zero delay. Contours below 15% of the maximum absolute signal for each spectrum are omitted for clarity.

procedure, the biexciton binding energy remains roughly independent of n and greater than 28.5 meV for all phases.

The broadband TA spectra of n = 3 and n = 4 microcrystals shown in Figure 2b,c also contain these same two spectral features. In n = 3, the GSB peak appears at 2.033 eV and the ESA peak at 1.975 eV, whereas in n = 4, the GSB peak is at 1.919 eV and the ESA is at 1.858 eV. After Lorentzian fitting, the extracted biexciton binding energy is 47.7 meV in n = 3and 56.9 meV in n = 4. The exciton binding energy of RP perovskites is known to decrease with increasing n, as has been confirmed by previous experimental work.²¹ It is expected that the biexciton binding energies should do the same. Indeed, simulations of biexcitons in 2D perovskites by Berkelbach and co-workers⁴¹ have suggested a decreasing biexciton binding energy and have found that the binding energy in n = 3 should be roughly k_BT at room temperature, making it surprising that we observe biexcitons in n = 3 and n = 4 at all, let alone with a roughly n independent binding energy. We further show the dynamics of the GSB and ESA peaks of the n = 2-4 RP perovskite microcrystals in Figure S2. Both the ESA and GSB peaks relax over a few picoseconds. No spectral evolution was observed within our 10 ps time window. The few picosecond lifetime of the ESA peak in all three n phases confirms the biexciton assignment to this feature as opposed to bandgap renormalization, which would be expected to have a lifetime of $<\!1~ps.^{63-65}$

We further used hyperspectral TA microscopy to map out the spectral response within individual microcrystals with submicron spatial resolution. Because we collect a full TA spectrum at each pixel, we can track variations in the position of the GSB and ESA peaks throughout the crystal. Shown in Figure 3a is a map of the position of the GSB peak, estimated as before from fitting, throughout a single crystal of n = 2 RP perovskite. We observe spatial variations in the exciton energy over a range of 60 meV. Further, distinct few micron regions of different energies can be observed within this single object (for example, the red region in the top center, or the two small blue regions immediately below). Similar variations of about 20 meV are seen in the position of the ESA peak (Figure 3b),

though the spatial pattern within this crystal is different than the variation of the GSB peak, indicating that excitons and biexcitons may sense the heterogeneity in this crystal differently. This point will be expanded on in later sections. Similar spatial variations in the GSB and ESA peaks are observed in microcrystals of n=3 (Figure 3e,f) and n=4 RP perovskites (Figure 3i,j). Optical microscopy indicates these microcrystals are single objects (Figure S1), yet, micron-scale spatial variations in the electronic structure of the exciton and biexciton are observed.

In Figure 3c,g,k, we plot the spatial variation of the biexciton binding energy, estimated from the Lorentzian fits to each TA spectrum. Common to all three images is an enhancement of the biexciton binding energy within 1–2 pixels of the crystal edge (each pixel is a 500 nm step). From these binding energy images, we calculate histograms, shown in Figure 3d,h,l. Again, we find a biexciton binding energy that is roughly independent of *n*. The widths of these distributions are around 20–30 meV, indicating significant structural heterogeneity in these microcrystals. We also observed some crystal-to-crystal variation in the amount of disorder present, but all crystals studied here had variations in biexciton binding energy on the order of 25 meV.

To more sensitively characterize the energetic landscape of the excitons and biexcitons in these materials, we turn to 2DWL spectroscopy. Briefly, 2DWL spectroscopy utilizes two pump pulses and a probe pulse, to spread the TA spectrum out onto a pump energy axis in addition to the probe energy axis, mapping out the full third-order response. Figure 4a shows the 2DWL spectrum at zero pump-probe delay for a microcrystal of n = 2 perovskite. Similar to the TA spectrum, we resolve two main features: a negative GSB and a positive ESA. The bleach of the exciton has a homogeneous lineshape, consistent with the Lorentzian lineshapes fit to the TA spectra. The diagonal peak corresponding to the bleach of the exciton extends as a streak to higher pump energies. This kind of lineshape is common in 2D spectra of semiconductors and arises from the coupling of states higher than the band edge (i.e., other points in momentum space) sharing a ground state with the band

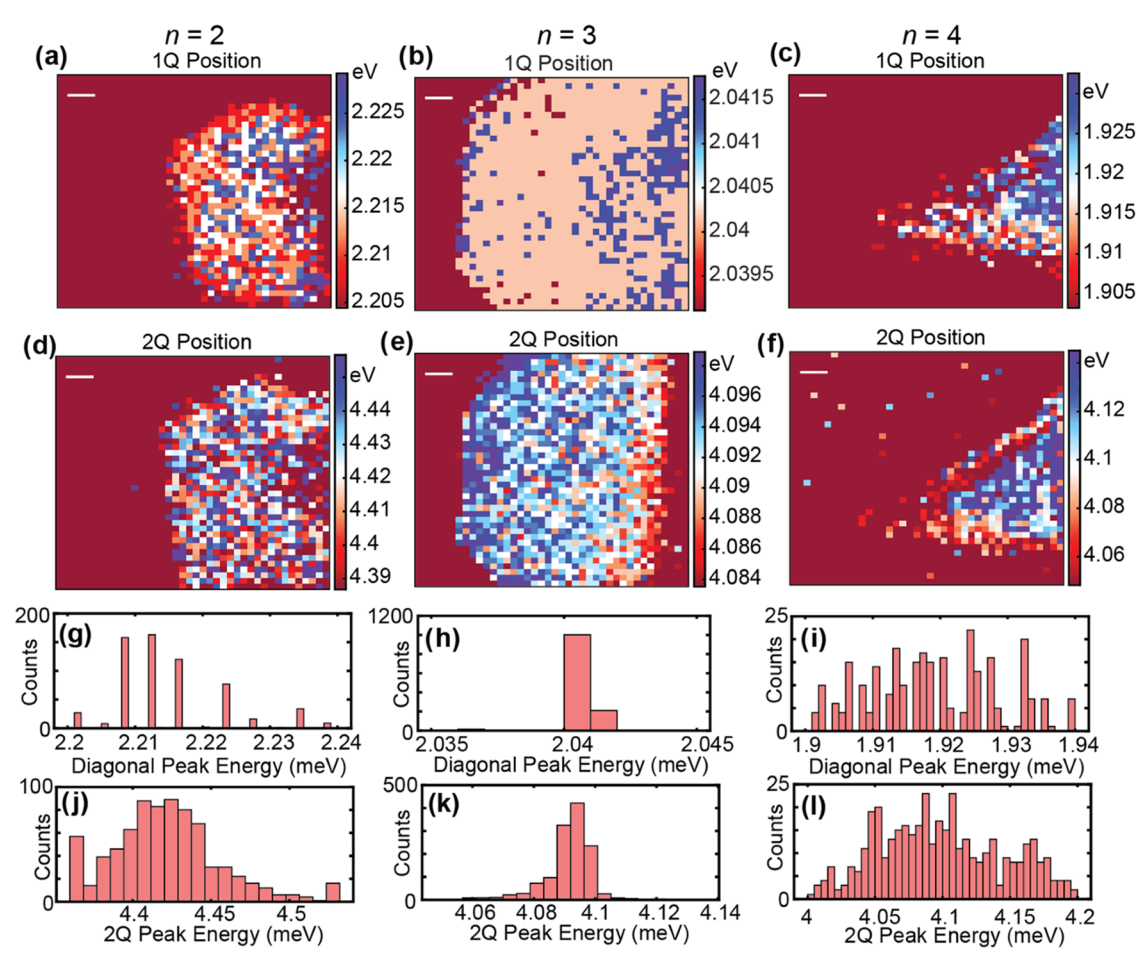


Figure 5. 2DWL microscopy $BA_2MA_{n-1}Pb_nI_{3n+1}$ microcrystals. The 1Q diagonal peak energy (a-c) and 2Q pump energy (d-f) are shown as a function of position for n = 2 (a, d), n = 3 (b, e), and n = 4 (c, f) perovskite microcrystals. Histograms of the 1Q (g-i) and 2Q (j-l) peak positions calculated from the images are also shown. All scale bars in the 2DWL images are 2 μ m.

edge. The ESA also appears as a streak at pump energies higher than the band. There is hardly any ESA when pumping directly at the band edge, and only pumping with excess energy leads to the observation of the ESA. This finding has been observed previously in CsPbI₃ nanocrystals^{66,67} using TA spectroscopy and in CdSe quantum dots using 2D electronic spectroscopy and has been assigned to be hot biexcitons. A hot biexciton can be thought of as an excited state of the biexciton system. Although the biexciton can be thought of as two band edge 1s excitons bound together, a hot biexciton may be composed of two different higher-energy excitons, such as 1s and 2s or 1s and 2p, or excitons of different types, such as heavy hole excitons and light hole excitons as in GaAs quantum wells.^{68–70} The 2DWL spectra of n = 3 and n = 4 perovskite microcrystals (Figure 4b,c) exhibit similar features as the spectrum for n = 2 perovskite microcrystals, with bleaching above the bandgap and an ESA present for pump energies higher than the band edge. It appears that the ESA feature peaks with more excess pump energy with increasing n. In n = n2, the ESA is peaked roughly 50 meV above the band edge, whereas in n = 3 and 4, this feature is peaked roughly 100 and 200 meV above the band edge, respectively. Due to the fixed bandwidth of our pulses, we are unable to tell if these differences are material related, or if they are an artifact of our observable spectral range. We also note that all our 2DWL experiments are conducted at zero pump-probe delay; thus, our experiments are not sensitive to the relaxation pathways of

these hot biexcitons, only their existence. Additionally, the 2DWL spectrum of n=4 perovskite contains a diagonal peak and extended higher-energy bleach from n=3 perovskite impurities within this microcrystal. There is nonzero bleach signal at the cross-peak location between these two diagonal peaks, but there is also much stronger cross-peak signal at higher pump energies, indicating that hot excitons may be able to transfer more efficiently from n=3 to n=4 perovskite layers than band edge excitons, but any further discussion of this feature is beyond the scope of the present work.

Both the TA and 2DWL spectra suffer from overlapping GSB and ESA peaks, complicating the independent analysis of these two features. Therefore, we turn to two-quantum (2Q) 2DWL spectroscopy to correlate the energies of the biexciton states to those of the exciton states. In a 2Q-2DWL experiment, additional light—matter interactions allow for the observations of cross-peaks between doubly excited states (such as biexcitons) and singly excited states (such as excitons). Indeed, the 2Q-2DWL spectrum could be viewed as an extension of the 1Q-2DWL spectrum to a higher pump energy range. The 2Q-2DWL pulse sequence is designed to measure biexcitons and has been used for that purpose many times in the past.

Recently, Farrell et al.⁷¹ developed the "permuted pumpprobe sequence" for measuring third- and fifth-order twoquantum Feynman pathways using a conventional 2D infrared spectrometer in the pump-probe geometry. We apply this pulse sequence in the collinear geometry and the visible spectral range. Details of the collection and processing of these spectra are given in the Supporting Information. The 2Q-2DWL spectrum of n = 2 perovskite (Figure 4d) shows several peaks and the two most intense sets of peaks are labeled the 0Q and the 2Q transition. The permuted pump-probe pulse sequence only measures the nonrephasing 2Q pathway, meaning that nonrephasing lineshapes are expected. Therefore, the sets of positive and negative peaks seen in each of the 2Q-2DWL spectra are from a single transition. The feature that is lower in energy along the 2Q pump axis is the 0Q peak, and shows up at the energy of twice the rotating frame applied with our pulse shaper (see the Supporting Information for more details). We do not analyze this feature to learn more about the properties of the material, but instead use it as a frequency reference to extract the 2Q frequencies. The 2Q transition shows up at pump energies above the 2Q diagonal (y = 2x) in all of the spectra shown here. Conventionally, this would indicate repulsive exciton–exciton interactions, as have been described in InAs and CdSe quantum dots.^{72–75} However, the 1Q-2DWL spectrum (Figure 4a) shows that the biexcitons in 2D perovskites are hot biexcitons, and the position of the 2Q peak confirms this. Indeed, other measurements of the 2O spectrum of mixed 2D perovskites have also exhibited peaks above the diagonal. 15 We find it interesting that the 2Q transitions are relatively narrow along the 2Q pump axis, which appears to be in contrast to the fact that the ESA signal in the 1Q-2DWL spectrum can be pumped over a relatively large energy range above the bandgap. Similar 2Q transitions above the 2Q diagonal are seen for n = 3 and n = 4 perovskites, also with relatively narrow linewidths. In the 2Q-2DWL spectrum for n= 4 perovskite (Figure 4f), we observe 2Q signal at the probe energy for n = 3 as well as n = 4 perovskite, suggesting that biexcitons exist in both layers. This cannot be gleaned from the 1Q-2DWL spectrum of n = 4 perovskite (Figure 4c) because of spectral congestion. Fluence-dependent PL experiments (see Figure S4) indicate that biexciton formation is relatively inefficient and that triexciton formation is completely negligible. Here, biexcitons are probed through the ESA feature that is created by both the pump and probe pulses. Meaning that biexciton generation depends on both the pump and probe fluences. Our phase cycling of the pump pulses for the 2DWL experiments excludes Feynman diagrams associated with triexcitons and higher many-body states (see Figure S4).

With the exciton energies taken from the 1Q-2DWL spectra and the biexciton energies taken from the 2Q-2DWL spectra, we can directly compare the spatial variations of the excitons and biexcitons within individual microcrystals. Figure 5a-f shows 2DWL images that contain a 1Q- and 2Q-2DWL spectrum at each pixel. Figure 5a-c shows images of the exciton energy, taken from the diagonal peak position in the 1Q-2DWL spectra, and the corresponding histograms of 1Q diagonal peak energy are shown in Figure 5g-i. Figure 5d-f shows images of the biexciton energy, taken from the 2Q-2DWL spectra, and the corresponding histograms of 2Q peak energy are shown in Figure 5j-l. We see that the 1Q diagonal peak energy does not vary substantially over a microcrystal, only a few meV, whereas the 2Q peak position varies much more drastically. We recall that the Lorentzian fits used to analyze the TA microscopy images in Figure 3 seem to indicate the excitons varied more drastically. However, the biexciton energies measured in the 2Q-2DWL spectra are completely deconvoluted from the exciton energies, whereas Lorentzian

fitting of the overlapping features in the TA or 1Q-2DWL spectra may only result in a partial deconvolution. The 2Q-2DWL images in Figure 5d—f show that biexcitons exhibit more spatial variations than excitons. We believe this difference is due to the different degrees of sensitivity of excitons and biexcitons to their environment. In the Discussion section, we will discuss the origins of this difference in sensitivity, as well as possible structural sources for the disorder experienced by the excitons and biexcitons.

DISCUSSION

pubs.acs.org/JACS

We have observed biexcitons in microcrystals of n = 2-4 RP perovskites. We find the binding energy is roughly independent of n with a value of roughly 60 meV. Significant spatial variations are observed in the energies of both the exciton and biexciton states within individual microcrystals. We hypothesize that static and dynamic disorder create the n independence of the biexciton binding energies and lead to the observed spatial variations. We discuss the possible structural origins of this disorder below.

Simple theories of exciton and biexciton binding have shown the carrier effective masses and the dielectric environment to be critical in determining if biexciton states are bound or unbound. Briefly, bound states are created through a competition between the kinetic and potential energy terms in the Hamiltonian. Bound states typically have less kinetic energy than unbound states. Changes to the carrier effective masses largely modify the carrier kinetic energies, while changes to the dielectric environment impact the potential energy terms. From a structural point of view, changes to the effective mass, created by strain, point defects, and scattering with phonons, are much more likely to occur than changes to the dielectric environment.

Changes to the effective mass imply changes to the underlying electronic structure of the material. These changes, representing a departure from the electronic structure of the pristine perovskite materials, may be caused by several structural factors including disorder in the octahedral layer, and disorder in the organic layer. All of these structural effects may be coupled, but we discuss them independently.

The structure of the octahedral layer of 2D perovskites, especially the angles between neighboring octahedra, is known to tune both the electron and hole effective masses.⁷⁶ While different spacer and or B cations may be used to tune the structure of the octahedral layer, static and dynamic disorder in the octahedral layer will also change these angles within a single microcrystal. The Pb-I stretching and I-Pb-I bending phonon modes (cage-rattling modes) of perovskites are thermally populated at room temperature, 77,78 meaning that the octahedral layer has a dynamic structure, and the electron and hole effective masses are also dynamic. This effect is a manifestation of electron-phonon coupling in these materials, which is known to be strong.8 The lineshapes of the 1Q-2DWL spectra are homogeneously broadened, which is consistent with fast fluctuations of the cage-rattling modes of the octahedral layers. This finding corroborates the idea that dynamic disorder may play a large role in tuning the carrier effective masses and thus the biexciton binding energies. Further, the lineshapes of the 2Q-2DWL spectra are also homogeneously broadened, albeit with nonrephasing lineshapes, complicating the assignment. These 2Q lineshapes further implicate the motion of the octahedral cage in tuning the biexciton binding energy.

Moreover, strain in the crystal can alter the local structure of the perovskite layers. We often observe higher biexciton binding energies near microcrystal edges, where strain is known to be more pronounced. The carrier effective masses are also known to depend on the identity and structure of the spacer cation in 2D perovskites.³² There is strong coupling between the end of the spacer cation and the surface of the octahedral layer, and through this coupling disorder in the organic layer is transmitted to the carriers residing in the octahedral layer. 31,32,79,80 While all of these effects may be playing a role in modulating the effective masses on micron length scales, we believe local variations in defect concentration and disorder in the octahedral layer to be most

All of our measurements were collected from multilayer crystals of RP perovskites that were 100-200 nm thick, introducing the possibility of interlayer interactions between neighboring octahedral layers. One simple explanation for the n independence of the biexciton binding energy is that the biexcitons in this system are interlayer biexcitons, meaning that the constituent excitons interact across the organic spacer layers. This spacer layer is constant for all RP perovskite phases considered here (BA cation), meaning that interlayer biexcitons would be separated by the same distance and the same dielectric environment regardless of the n phase. Previous theoretical models of biexcitons in 2D perovskites, 40,41 including the model described in this work, have not captured exciton interactions between different perovskite layers, which could explain their prediction of a decreasing biexciton binding energy for increasing n. Though our experiments do not provide any direct evidence for such interlayer biexcitons, comparative measurements of the biexciton binding energies in 2D perovskites with different spacer cations could help support this idea in the future.

We have observed efficient generation of hot biexcitons at pump energies higher than the band edge (Figure 4). Hot biexcitons have been observed before in both CsPbI3 nanocrystals^{66,67} and CdSe quantum dots.⁶¹ In 2D perovskites, the hot biexciton is likely composed of a 1s exciton at the band edge, and a higher-energy exciton such as a 2s or 2p exciton. Mixed biexcitons such as these were first described in ZnSe, 81 InGaAs, $^{\rm 82}$ and GaAs, $^{\rm 69}$ where biexcitons could be formed from a heavy hole exciton and a light hole exciton. They were also observed in CuCl crystals⁶⁸ and quantum dots,⁷⁰ with transitions from the 1s-1s biexciton to the 1s-2s biexciton observed using infrared transient absorption. Because we have not collected 2DWL spectra after $t_2 = 0$, we are unable to determine if these $1s-n\bar{l}$ (n > 1) biexcitons relax to the 1s-1sbiexciton ground state before recombining, or if they recombine directly from the initial hot state. But the transient absorption data shown in Figure S2 shows that the ESA associated with biexcitons has a few-ps lifetime, indicating that cooling of these mixed biexciton states may be quite slow.

Spatially varying exciton and biexciton energies observed herein, induced by varying electron and hole effective masses, have huge implications for the performance of 2D perovskitebased optoelectronic devices. Disorder in the energies and mobilities of charge carriers impacts transport efficiencies and can result in greater losses to recombination. Stable biexcitons in all of the n phases studied here can enhance Auger recombination, which is particularly detrimental to high carrier density applications such as lasing. Furthermore, we have shown that biexcitons can be more sensitive to their environment than excitons, meaning that biexcitons may be a general probe of structural disorder in other materials.

CONCLUSIONS

We have used multiquantum 2DWL microscopy to study the spatial variations of excitons and biexcitons within individual microcrystals of n = 2-4 2D RP perovskites $BA_2MA_{n-1}Pb_nI_{3n+1}$. These experiments as well as TA and PL experiments show that stable hot biexcitons exist in all of these phases and the average biexciton binding energy of around 60 meV is essentially independent of the perovskite layer thickness (n). The spatial variations are caused by large static and dynamics disorder since different parts of the crystal may be disordered to varying extents. The disorder likely arises from the disorder of the octahedral layers and local variations in point defect concentration in RP perovskites, suggesting that biexcitons may be used as a sensitive probe of these effects in semiconductor materials in general. These results demonstrate that disorder in crystalline semiconductors can lead to significant deviations between the photophysical properties of a disordered material and what is predicted for an ideal crystal. These first 2DWL microscopy experiments on 2D RP perovskites reveal previously unknown insights about the spatial heterogeneity of the energetic landscape of excitons and biexcitons.

ASSOCIATED CONTENT

Supporting Information

The Supporting Information is available free of charge at https://pubs.acs.org/doi/10.1021/jacs.3c05533.

Detailed experimental methods, optical microscopy images, and transient absorption dynamics (PDF)

AUTHOR INFORMATION

Corresponding Authors

Song Jin – Department of Chemistry, University of Wisconsin-Madison, Madison, Wisconsin 53706, United States; orcid.org/0000-0001-8693-7010; Email: jin@ chem.wisc.edu

Martin T. Zanni – Department of Chemistry, University of Wisconsin-Madison, Madison, Wisconsin 53706, United States; o orcid.org/0000-0001-7191-9768; Email: zanni@ chem.wisc.edu

Authors

Zachary T. Armstrong – Department of Chemistry, University of Wisconsin-Madison, Madison, Wisconsin 53706, United States; o orcid.org/0000-0002-1207-6171

Kristel M. Forlano – Department of Chemistry, University of Wisconsin-Madison, Madison, Wisconsin 53706, United States; orcid.org/0000-0001-6200-091X

Chris R. Roy – Department of Chemistry, University of Wisconsin-Madison, Madison, Wisconsin 53706, United States; orcid.org/0000-0001-6438-9543

Miriam Bohlmann Kunz – Department of Chemistry, University of Wisconsin-Madison, Madison, Wisconsin 53706, United States; oorcid.org/0000-0002-7852-159X

Kieran Farrell - Department of Chemistry, University of Wisconsin-Madison, Madison, Wisconsin 53706, United States

- Dongxu Pan Department of Chemistry, University of Wisconsin-Madison, Madison, Wisconsin 53706, United States
- John C. Wright Department of Chemistry, University of Wisconsin-Madison, Madison, Wisconsin 53706, United States; orcid.org/0000-0002-6926-1837

Complete contact information is available at: https://pubs.acs.org/10.1021/jacs.3c05533

Notes

The authors declare the following competing financial interest(s): M.T.Z. is a co-owner of PhaseTech Spectroscopy, which sells ultrafast pulse shapers and spectrometers.

ACKNOWLEDGMENTS

Funding for this research was provided by the National Science Foundation under Award Number 1954700 (TA, 2DWL microscopy, Z.T.A., M.B.K., K.F., M.T.Z.) and the Department of Energy Office of Basic Energy Sciences, Division of Materials Sciences and Engineering, under Award DE-SC0002162 (synthesis and structural characterization of materials, K.M.F., C.R.R., D.P., J.C.W., S.J.). K.M.F. acknowledges support from the NSF GRFP under Award Number 1747503. M.T.Z. is a co-owner of PhaseTech Spectroscopy, which sells ultrafast pulse shapers and spectrometers.

REFERENCES

- (1) Li, X.; Hoffman, J. M.; Kanatzidis, M. G. The 2D Halide Perovskite Rulebook: How the Spacer Influences Everything from the Structure to Optoelectronic Device Efficiency. *Chem. Rev.* **2021**, *121*, 2230–2291.
- (2) Mauck, C. M.; Tisdale, W. A. Excitons in 2D Organic—Inorganic Halide Perovskites. *Trends Chem.* **2019**, *1*, 380–393.
- (3) Blancon, J.-C.; Even, J.; Stoumpos, C. C.; Kanatzidis, M. G.; Mohite, A. D. Semiconductor Physics of Organic–Inorganic 2D Halide Perovskites. *Nat. Nanotechnol.* **2020**, *15*, 969–985.
- (4) Fu, Y.; Zhu, H.; Chen, J.; Hautzinger, M. P.; Zhu, X.-Y.; Jin, S. Metal Halide Perovskite Nanostructures for Optoelectronic Applications and the Study of Physical Properties. *Nat. Rev. Mater.* **2019**, *4*, 169–188.
- (5) Dohner, E. R.; Hoke, E. T.; Karunadasa, H. I. Self-Assembly of Broadband White-Light Emitters. *J. Am. Chem. Soc.* **2014**, *136*, 1718–1721.
- (6) Crace, E. J.; Su, A. C.; Karunadasa, H. I. Reliably Obtaining White Light from Layered Halide Perovskites at Room Temperature. *Chem. Sci.* **2022**, *13*, 9973–9979.
- (7) Thouin, F.; Valverde-Chávez, D. A.; Quarti, C.; Cortecchia, D.; Bargigia, I.; Beljonne, D.; Petrozza, A.; Silva, C.; Kandada, A. R. S. Phonon Coherences Reveal the Polaronic Character of Excitons in Two-Dimensional Lead Halide Perovskites. *Nat. Mater.* **2019**, *18*, 349–356.
- (8) Thouin, F.; Kandada, A. R. S.; Valverde-Chávez, D. A.; Cortecchia, D.; Bargigia, I.; Petrozza, A.; Yang, X.; Bittner, E. R.; Silva, C. Electron—Phonon Couplings Inherent in Polarons Drive Exciton Dynamics in Two-Dimensional Metal-Halide Perovskites. *Chem. Mater.* **2019**, *31*, 7085—7091.
- (9) Kandada, A. R. S.; Silva, C. Exciton Polarons in Two-Dimensional Hybrid Metal-Halide Perovskites. *J. Phys. Chem. Lett.* **2020**, *11*, 3173–3184.
- (10) Kondo, T.; Azuma, T.; Yuasa, T.; Ito, R. Biexciton Lasing in the Layered Perovskite-Type Material (C6H13NH3)2PbI4. *Solid State Commun.* 1998, 105, 253–255.
- (11) Raghavan, C. M.; Chen, T.-P.; Li, S.-S.; Chen, W.-L.; Lo, C.-Y.; Liao, Y.-M.; Haider, G.; Lin, C.-C.; Chen, C.-C.; Sankar, R.; Chang, Y.-M.; Chou, F.-C.; Chen, C.-W. Low-Threshold Lasing from 2D

- Homologous Organic—Inorganic Hybrid Ruddlesden—Popper Perovskite Single Crystals. *Nano Lett.* **2018**, *18*, 3221—3228.
- (12) He, X.; Gong, H.; Huang, H.; Li, Y.; Ren, J.; Li, Y.; Liao, Q.; Gao, T.; Fu, H. Multicolor Biexciton Lasers Based on 2D Perovskite Single Crystalline Flakes. *Adv. Opt. Mater.* **2022**, *10*, No. 2200238.
- (13) Thouin, F.; Neutzner, S.; Cortecchia, D.; Dragomir, V. A.; Soci, C.; Salim, T.; Lam, Y. M.; Leonelli, R.; Petrozza, A.; Kandada, A. R. S.; Silva, C. Stable Biexcitons in Two-Dimensional Metal-Halide Perovskites with Strong Dynamic Lattice Disorder. *Phys. Rev. Mater.* **2018**, *2*, No. 034001.
- (14) Huang, X.; Chen, L.; Zhang, C.; Qin, Z.; Yu, B.; Wang, X.; Xiao, M. Inhomogeneous Biexciton Binding in Perovskite Semi-conductor Nanocrystals Measured with Two-Dimensional Spectroscopy. *J. Phys. Chem. Lett.* **2020**, *11*, 10173–10181.
- (15) Elkins, M. H.; Pensack, R.; Proppe, A. H.; Voznyy, O.; Quan, L. N.; Kelley, S. O.; Sargent, E. H.; Scholes, G. D. Biexciton Resonances Reveal Exciton Localization in Stacked Perovskite Quantum Wells. *J. Phys. Chem. Lett.* **2017**, *8*, 3895–3901.
- (16) Fu, Y. Stabilization of Metastable Halide Perovskite Lattices in the 2D Limit. *Adv. Mater.* **2022**, *34*, No. 2108556.
- (17) Fu, Y.; Hautzinger, M. P.; Luo, Z.; Wang, F.; Pan, D.; Aristov, M. M.; Guzei, I. A.; Pan, A.; Zhu, X.; Jin, S. Incorporating Large A Cations into Lead Iodide Perovskite Cages: Relaxed Goldschmidt Tolerance Factor and Impact on Exciton—Phonon Interaction. ACS Cent. Sci. 2019, 5, 1377—1386.
- (18) Hautzinger, M. P.; Pan, D.; Pigg, A. K.; Fu, Y.; Morrow, D. J.; Leng, M.; Kuo, M.-Y.; Spitha, N.; Lafayette, D. P. I.; Kohler, D. D.; Wright, J. C.; Jin, S. Band Edge Tuning of Two-Dimensional Ruddlesden—Popper Perovskites by A Cation Size Revealed through Nanoplates. ACS Energy Lett. 2020, 5, 1430—1437.
- (19) Pan, D.; Fu, Y.; Spitha, N.; Zhao, Y.; Roy, C. R.; Morrow, D. J.; Kohler, D. D.; Wright, J. C.; Jin, S. Deterministic Fabrication of Arbitrary Vertical Heterostructures of Two-Dimensional Ruddlesden—Popper Halide Perovskites. *Nat. Nanotechnol.* **2021**, *16*, 159—165.
- (20) Roy, C. R.; Zhou, Y.; Kohler, D. D.; Zhu, Z.; Wright, J. C.; Jin, S. Intrinsic Halide Immiscibility in 2D Mixed-Halide Ruddlesden—Popper Perovskites. *ACS Energy Lett.* **2022**, *7*, 3423—3431.
- (21) Blancon, J.-C.; Stier, A. V.; Tsai, H.; Nie, W.; Stoumpos, C. C.; Traoré, B.; Pedesseau, L.; Kepenekian, M.; Katsutani, F.; Noe, G. T.; Kono, J.; Tretiak, S.; Crooker, S. A.; Katan, C.; Kanatzidis, M. G.; Crochet, J. J.; Even, J.; Mohite, A. D. Scaling Law for Excitons in 2D Perovskite Quantum Wells. *Nat. Commun.* **2018**, *9*, No. 2254.
- (22) Miyata, A.; Mitioglu, A.; Plochocka, P.; Portugall, O.; Wang, J. T.-W.; Stranks, S. D.; Snaith, H. J.; Nicholas, R. J. Direct Measurement of the Exciton Binding Energy and Effective Masses for Charge Carriers in Organic–Inorganic Tri-Halide Perovskites. *Nat. Phys.* 2015, *11*, 582–587.
- (23) Kahmann, S.; Duim, H.; Rommens, A. J.; Tekelenburg, E. K.; Shao, S.; Loi, M. A. Grain-Specific Transitions Determine the Band Edge Luminescence in Dion—Jacobson Type 2D Perovskites. *Adv. Opt. Mater.* **2021**, *9*, No. 2100892.
- (24) Seitz, M.; Meléndez, M.; Alcázar-Cano, N.; Congreve, D. N.; Delgado-Buscalioni, R.; Prins, F. Mapping the Trap-State Landscape in 2D Metal-Halide Perovskites Using Transient Photoluminescence Microscopy. *Adv. Opt. Mater.* **2021**, *9*, No. 2001875.
- (25) Williams, O. F.; Zhou, N.; Hu, J.; Ouyang, Z.; Kumbhar, A.; You, W.; Moran, A. M. Imaging Excited State Dynamics in Layered 2D Perovskites with Transient Absorption Microscopy. *J. Phys. Chem.* A **2019**, *123*, 11012–11021.
- (26) Liang, M.; Lin, W.; Zhao, Q.; Li, J.; Zhu, L.; Sarpi, B.; Zakharov, A.; Scheblykin, I. G.; Pullerits, T.; Niu, Y.; Canton, S. E.; Zheng, K. Spatially Resolved Local Electronic Properties of 2D Lead Halide Perovskite Single Crystals Studied by X-Ray Photoemission Electron Microscopy. *Sol. RRL* **2023**, *7*, No. 2200795.
- (27) Frohna, K.; Anaya, M.; Macpherson, S.; Sung, J.; Doherty, T. A. S.; Chiang, Y.-H.; Winchester, A. J.; Orr, K. W. P.; Parker, J. E.; Quinn, P. D.; Dani, K. M.; Rao, A.; Stranks, S. D. Nanoscale Chemical

- Heterogeneity Dominates the Optoelectronic Response of Alloyed Perovskite Solar Cells. *Nat. Nanotechnol.* **2022**, *17*, 190–196.
- (28) Ghosh, S.; Pradhan, B.; Zhang, Y.; Roeffaers, M. B. J.; Hofkens, J.; Karki, K. J.; Materny, A. Spatial Heterogeneity of N-Phases Leads to Different Photophysical Properties in Quasi-Two-Dimensional Methylammonium Lead Bromide Perovskite. *J. Phys. Chem. C* 2022, 126, 478–486.
- (29) Xi, J.; Byeon, J.; Kim, U.; Bang, K.; Han, G. R.; Kim, J.-Y.; Yoon, J.; Dong, H.; Wu, Z.; Divitini, G.; Xi, K.; Park, J.; Lee, T.-W.; Keun Kim, S.; Choi, M.; Woo Lee, J. Abnormal Spatial Heterogeneity Governing the Charge-Carrier Mechanism in Efficient Ruddlesden—Popper Perovskite Solar Cells. *Energy Environ. Sci.* **2021**, *14*, 4915—4925.
- (30) Wang, J.; Zhu, J.; Jiang, Y.; Li, M.; Yu, K.; Wang, G. P. Observation of Elastic Heterogeneity and Phase Evolution in 2D Layered Perovskites Using Coherent Acoustic Phonons. *Nanophotonics* **2021**, *10*, 4009–4017.
- (31) Straus, D. B.; Iotov, N.; Gau, M. R.; Zhao, Q.; Carroll, P. J.; Kagan, C. R. Longer Cations Increase Energetic Disorder in Excitonic 2D Hybrid Perovskites. *J. Phys. Chem. Lett.* **2019**, *10*, 1198–1205.
- (32) Li, C.; Yang, J.; Su, F.; Tan, J.; Luo, Y.; Ye, S. Conformational Disorder of Organic Cations Tunes the Charge Carrier Mobility in Two-Dimensional Organic-Inorganic Perovskites. *Nat. Commun.* **2020**, *11*, No. 5481.
- (33) Guo, Z.; Wu, X.; Zhu, T.; Zhu, X.; Huang, L. Electron-Phonon Scattering in Atomically Thin 2D Perovskites. *ACS Nano* **2016**, *10*, 9992–9998.
- (34) Wang, S.; Ma, J.; Li, W.; Wang, J.; Wang, H.; Shen, H.; Li, J.; Wang, J.; Luo, H.; Li, D. Temperature-Dependent Band Gap in Two-Dimensional Perovskites: Thermal Expansion Interaction and Electron-Phonon Interaction. *J. Phys. Chem. Lett.* **2019**, *10*, 2546–2553.
- (35) Straus, D. B.; Hurtado Parra, S.; Iotov, N.; Gebhardt, J.; Rappe, A. M.; Subotnik, J. E.; Kikkawa, J. M.; Kagan, C. R. Direct Observation of Electron—Phonon Coupling and Slow Vibrational Relaxation in Organic—Inorganic Hybrid Perovskites. *J. Am. Chem. Soc.* **2016**, *138*, 13798—13801.
- (36) Du, Q.; Zhu, C.; Yin, Z.; Na, G.; Cheng, C.; Han, Y.; Liu, N.; Niu, X.; Zhou, H.; Chen, H.; Zhang, L.; Jin, S.; Chen, Q. Stacking Effects on Electron—Phonon Coupling in Layered Hybrid Perovskites via Microstrain Manipulation. *ACS Nano* **2020**, *14*, 5806—5817.
- (37) Jana, M. K.; Song, R.; Liu, H.; Khanal, D. R.; Janke, S. M.; Zhao, R.; Liu, C.; Valy Vardeny, Z.; Blum, V.; Mitzi, D. B. Organic-to-Inorganic Structural Chirality Transfer in a 2D Hybrid Perovskite and Impact on Rashba-Dresselhaus Spin-Orbit Coupling. *Nat. Commun.* **2020**, *11*, No. 4699.
- (38) Yang, J.-J.; Chen, W.-K.; Liu, X.-Y.; Fang, W.-H.; Cui, G. Spin—Orbit Coupling Is the Key to Promote Asynchronous Photoinduced Charge Transfer of Two-Dimensional Perovskites. *JACS Au* **2021**, *1*, 1178–1186.
- (39) Amat, A.; Mosconi, E.; Ronca, E.; Quarti, C.; Umari, P.; Nazeeruddin, Md. K.; Grätzel, M.; De Angelis, F. Cation-Induced Band-Gap Tuning in Organohalide Perovskites: Interplay of Spin—Orbit Coupling and Octahedra Tilting. *Nano Lett.* **2014**, *14*, 3608—3616.
- (40) Cho, Y.; Berkelbach, T. C. Optical Properties of Layered Hybrid Organic—Inorganic Halide Perovskites: A Tight-Binding GW-BSE Study. *J. Phys. Chem. Lett.* **2019**, *10*, 6189–6196.
- (41) Cho, Y.; Greene, S. M.; Berkelbach, T. C. Simulations of Trions and Biexcitons in Layered Hybrid Organic-Inorganic Lead Halide Perovskites. *Phys. Rev. Lett.* **2021**, *126*, No. 216402.
- (42) Ashner, M. N.; Shulenberger, K. E.; Krieg, F.; Powers, E. R.; Kovalenko, M. V.; Bawendi, M. G.; Tisdale, W. A. Size-Dependent Biexciton Spectrum in CsPbBr3 Perovskite Nanocrystals. *ACS Energy Lett.* **2019**, *4*, 2639–2645.
- (43) Castañeda, J. A.; Nagamine, G.; Yassitepe, E.; Bonato, L. G.; Voznyy, O.; Hoogland, S.; Nogueira, A. F.; Sargent, E. H.; Cruz, C. H. B.; Padilha, L. A. Efficient Biexciton Interaction in Perovskite

- Quantum Dots Under Weak and Strong Confinement. ACS Nano 2016, 10, 8603-8609.
- (44) Aneesh, J.; Swarnkar, A.; Ravi, V. K.; Sharma, R.; Nag, A.; Adarsh, K. V. Ultrafast Exciton Dynamics in Colloidal CsPbBr3 Perovskite Nanocrystals: Biexciton Effect and Auger Recombination. *J. Phys. Chem. C* **2017**, *121*, 4734–4739.
- (45) Park, Y.-S.; Bae, W. K.; Pietryga, J. M.; Klimov, V. I. Auger Recombination of Biexcitons and Negative and Positive Trions in Individual Quantum Dots. *ACS Nano* **2014**, *8*, 7288–7296.
- (46) Zavelani-Rossi, M.; Lupo, M. G.; Tassone, F.; Manna, L.; Lanzani, G. Suppression of Biexciton Auger Recombination in CdSe/CdS Dot/Rods: Role of the Electronic Structure in the Carrier Dynamics. *Nano Lett.* **2010**, *10*, 3142–3150.
- (47) Eperon, G. E.; Jedlicka, E.; Ginger, D. S. Biexciton Auger Recombination Differs in Hybrid and Inorganic Halide Perovskite Quantum Dots. J. Phys. Chem. Lett. 2018, 9, 104–109.
- (48) Spitha, N.; Kohler, D. D.; Hautzinger, M. P.; Li, J.; Jin, S.; Wright, J. C. Discerning between Exciton and Free-Carrier Behaviors in Ruddlesden—Popper Perovskite Quantum Wells through Kinetic Modeling of Photoluminescence Dynamics. *J. Phys. Chem. C* **2020**, 124. 17430—17439.
- (49) Gao, L.; Zhang, F.; Xiao, C.; Chen, X.; Larson, B. W.; Berry, J. J.; Zhu, K. Improving Charge Transport via Intermediate-Controlled Crystal Growth in 2D Perovskite Solar Cells. *Adv. Funct. Mater.* **2019**, 29, No. 1901652.
- (50) Yang, Y.; Liu, C.; Syzgantseva, O. A.; Syzgantseva, M. A.; Ma, S.; Ding, Y.; Cai, M.; Liu, X.; Dai, S.; Nazeeruddin, M. K. Defect Suppression in Oriented 2D Perovskite Solar Cells with Efficiency over 18% via Rerouting Crystallization Pathway. *Adv. Energy Mater.* **2021**, *11*, No. 2002966.
- (51) Zhang, Z.; Fang, W.-H.; Long, R.; Prezhdo, O. V. Exciton Dissociation and Suppressed Charge Recombination at 2D Perovskite Edges: Key Roles of Unsaturated Halide Bonds and Thermal Disorder. J. Am. Chem. Soc. 2019, 141, 15557–15566.
- (52) Nishida, J.; Breen, J. P.; Lindquist, K. P.; Umeyama, D.; Karunadasa, H. I.; Fayer, M. D. Dynamically Disordered Lattice in a Layered Pb-I-SCN Perovskite Thin Film Probed by Two-Dimensional Infrared Spectroscopy. *J. Am. Chem. Soc.* **2018**, *140*, 9882–9890.
- (53) Kang, J.; Wang, L.-W. Dynamic Disorder and Potential Fluctuation in Two-Dimensional Perovskite. *J. Phys. Chem. Lett.* **2017**, *8*, 3875–3880.
- (54) Seiler, H.; Palato, S.; Sonnichsen, C.; Baker, H.; Socie, E.; Strandell, D. P.; Kambhampati, P. Two-Dimensional Electronic Spectroscopy Reveals Liquid-like Lineshape Dynamics in CsPbI 3 Perovskite Nanocrystals. *Nat. Commun.* **2019**, *10*, No. 4962.
- (55) Gao, Y.; Shi, E.; Deng, S.; Shiring, S. B.; Snaider, J. M.; Liang, C.; Yuan, B.; Song, R.; Janke, S. M.; Liebman-Peláez, A.; Yoo, P.; Zeller, M.; Boudouris, B. W.; Liao, P.; Zhu, C.; Blum, V.; Yu, Y.; Savoie, B. M.; Huang, L.; Dou, L. Molecular Engineering of Organic—Inorganic Hybrid Perovskites Quantum Wells. *Nat. Chem.* **2019**, *11*, 1151–1157.
- (56) Deng, S.; Shi, E.; Yuan, L.; Jin, L.; Dou, L.; Huang, L. Long-Range Exciton Transport and Slow Annihilation in Two-Dimensional Hybrid Perovskites. *Nat. Commun.* **2020**, *11*, No. 664.
- (57) Jones, A. C.; Kearns, N. M.; Ho, J.-J.; Flach, J. T.; Zanni, M. T. Impact of Non-Equilibrium Molecular Packings on Singlet Fission in Microcrystals Observed Using 2D White-Light Microscopy. *Nat. Chem.* **2020**, *12*, 40–47.
- (58) Armstrong, Z. T.; Kunz, M. B.; Jones, A. C.; Zanni, M. T. Thermal Annealing of Singlet Fission Microcrystals Reveals the Benefits of Charge Transfer Couplings and Slip-Stacked Packing. *J. Phys. Chem. C* **2020**, *124*, 15123–15131.
- (59) Moody, G.; Singh, R.; Li, H.; Akimov, I. A.; Bayer, M.; Reuter, D.; Wieck, A. D.; Bracker, A. S.; Gammon, D.; Cundiff, S. T. Influence of Confinement on Biexciton Binding in Semiconductor Quantum Dot Ensembles Measured with Two-Dimensional Spectroscopy. *Phys. Rev. B* **2013**, *87*, No. 041304.
- (60) Hao, K.; Specht, J. F.; Nagler, P.; Xu, L.; Tran, K.; Singh, A.; Dass, C. K.; Schüller, C.; Korn, T.; Richter, M.; Knorr, A.; Li, X.;

- Moody, G. Neutral and Charged Inter-Valley Biexcitons in Monolayer MoSe2. Nat. Commun. 2017, 8, No. 15552.
- (61) Seiler, H.; Palato, S.; Sonnichsen, C.; Baker, H.; Kambhampati, P. Seeing Multiexcitons through Sample Inhomogeneity: Band-Edge Biexciton Structure in CdSe Nanocrystals Revealed by Two-Dimensional Electronic Spectroscopy. Nano Lett. 2018, 18, 2999-
- (62) Shukla, A.; Kaur, G.; Babu, K. J.; Ghorai, N.; Goswami, T.; Kaur, A.; Ghosh, H. N. Effect of Confinement on the Exciton and Biexciton Dynamics in Perovskite 2D-Nanosheets and 3D-Nanocrystals. J. Phys. Chem. Lett. 2020, 11, 6344-6352.
- (63) Fan, K.; Chan, C. C. S.; Yuan, L.; Yan, K.; Wong, K. S. New Insights into Hot-Charge Relaxation in Lead Halide Perovskite: Dynamical Bandgap Change, Hot-Biexciton Effect, and Photo-Bleaching Shift. ACS Photonics 2022, 9, 2304-2314.
- (64) Price, M. B.; Butkus, J.; Jellicoe, T. C.; Sadhanala, A.; Briane, A.; Halpert, J. E.; Broch, K.; Hodgkiss, J. M.; Friend, R. H.; Deschler, F. Hot-Carrier Cooling and Photoinduced Refractive Index Changes in Organic-Inorganic Lead Halide Perovskites. Nat. Commun. 2015, 6, No. 8420.
- (65) Trinh, M. T.; Wu, X.; Niesner, D.; Zhu, X.-Y. Many-Body Interactions in Photo-Excited Lead Iodide Perovskite. J. Mater. Chem. A 2015, 3, 9285-9290.
- (66) Kobiyama, E.; Tahara, H.; Sato, R.; Saruyama, M.; Teranishi, T.; Kanemitsu, Y. Reduction of Optical Gain Threshold in CsPbI3 Nanocrystals Achieved by Generation of Asymmetric Hot-Biexcitons. Nano Lett. 2020, 20, 3905-3910.
- (67) Yumoto, G.; Tahara, H.; Kawawaki, T.; Saruyama, M.; Sato, R.; Teranishi, T.; Kanemitsu, Y. Hot Biexciton Effect on Optical Gain in CsPbI3 Perovskite Nanocrystals. J. Phys. Chem. Lett. 2018, 9, 2222-2228.
- (68) Yoshioka, T.; Miyajima, K.; Ashida, M.; Itoh, T. Infrared Transient Absorption Spectra for Excited Transition of Excitons and Biexcitons in CuCl. Phys. Status Solidi C 2009, 6, 296-299.
- (69) Stone, K. W.; Gundogdu, K.; Turner, D. B.; Li, X.; Cundiff, S. T.; Nelson, K. A. Two-Quantum 2D FT Electronic Spectroscopy of Biexcitons in GaAs Quantum Wells. Science 2009, 324, 1169-1173.
- (70) Miyajima, K.; Edamatsu, K.; Itoh, T. Infrared Transient Absorption and Excited-States of Excitons and Biexcitons Confined in CuCl Quantum Dots. J. Lumin. 2004, 108, 371-374.
- (71) Farrell, K. M.; Zanni, M. T. Phase Stable, Shot-to-Shot Measurement of Third- and Fifth-Order Two-Quantum Correlation Spectra Using a Pulse Shaper in the Pump-Probe Geometry. J. Chem. Phys. 2022, 157, No. 014203.
- (72) Rodt, S.; Heitz, R.; Schliwa, A.; Sellin, R. L.; Guffarth, F.; Bimberg, D. Repulsive Exciton-Exciton Interaction in Quantum Dots. Phys. Rev. B 2003, 68, No. 035331.
- (73) Saba, M.; Minniberger, S.; Quochi, F.; Roither, J.; Marceddu, M.; Gocalinska, A.; Kovalenko, M. V.; Talapin, D. V.; Heiss, W.; Mura, A.; Bongiovanni, G. Exciton-Exciton Interaction and Optical Gain in Colloidal CdSe/CdS Dot/Rod Nanocrystals. Adv. Mater. 2009, 21, 4942-4946.
- (74) Cihan, A. F.; Kelestemur, Y.; Guzelturk, B.; Yerli, O.; Kurum, U.; Yaglioglu, H. G.; Elmali, A.; Demir, H. V. Attractive versus Repulsive Excitonic Interactions of Colloidal Quantum Dots Control Blue- to Red-Shifting (and Non-Shifting) Amplified Spontaneous Emission. J. Phys. Chem. Lett. 2013, 4, 4146-4152.
- (75) Vörös, Z.; Snoke, D. W.; Pfeiffer, L.; West, K. Direct Measurement of Exciton-Exciton Interaction Energy. Phys. Rev. Lett. 2009, 103, No. 016403.
- (76) Dyksik, M.; Duim, H.; Zhu, X.; Yang, Z.; Gen, M.; Kohama, Y.; Adjokatse, S.; Maude, D. K.; Loi, M. A.; Egger, D. A.; Baranowski, M.; Plochocka, P. Broad Tunability of Carrier Effective Masses in Two-Dimensional Halide Perovskites. ACS Energy Lett. 2020, 5, 3609-3616.
- (77) Quarti, C.; Grancini, G.; Mosconi, E.; Bruno, P.; Ball, J. M.; Lee, M. M.; Snaith, H. J.; Petrozza, A.; De Angelis, F. The Raman Spectrum of the CH3NH3PbI3 Hybrid Perovskite: Interplay of Theory and Experiment. J. Phys. Chem. Lett. 2014, 5, 279-284.

- (78) Dahod, N. S.; France-Lanord, A.; Paritmongkol, W.; Grossman, J. C.; Tisdale, W. A. Low-Frequency Raman Spectrum of 2D Layered Perovskites: Local Atomistic Motion or Superlattice Modes? J. Chem. Phys. 2020, 153, No. 044710.
- (79) Mauck, C. M.; France-Lanord, A.; Hernandez Oendra, A. C.; Dahod, N. S.; Grossman, J. C.; Tisdale, W. A. Inorganic Cage Motion Dominates Excited-State Dynamics in 2D-Layered Perovskites (CxH2x+1NH3)2PbI4 (x = 4-9). J. Phys. Chem. C 2019, 123, 27904-27916.
- (80) Passarelli, J. V.; Mauck, C. M.; Winslow, S. W.; Perkinson, C. F.; Bard, J. C.; Sai, H.; Williams, K. W.; Narayanan, A.; Fairfield, D. J.; Hendricks, M. P.; Tisdale, W. A.; Stupp, S. I. Tunable Exciton Binding Energy in 2D Hybrid Layered Perovskites through Donor-Acceptor Interactions within the Organic Layer. Nat. Chem. 2020, 12, 672-
- (81) Wagner, H. P.; Langbein, W.; Hvam, J. M. Mixed Biexcitons in Single Quantum Wells. Phys. Rev. B 1999, 59, 4584-4587.
- (82) Kim, K.; Norris, T. B.; Hohenester, U. Redshift of the Excited State Due to a Nondegenerate Biexciton in Self-Organized Quantum Dots. J. Appl. Phys. 2008, 103, No. 113702.